Effects of Radial Appendage Flexibility on Shaft Whirl Stability

F.J. Wilgen* and A.L. Schlack Jr.†
University of Wisconsin, Madison, Wis.

Introduction

THE move to lighter, more flexible gas turbine engine components has initiated several recent investigations into the effects of component flexibility on shaft whirl. Based on a study of a flexible shaft-disk model, Chivens and Nelson[1] concluded that critical speeds are not affected significantly by disk flexibility. Some limitations concerning this conclusion have been discussed by Klompas.[1,2]

The object of this Note is to show that, provided that a sufficiently wide range of parameters is considered, the effects of an appendage's flexibility on critical speeds can become significant. Critical speed stability boundaries are shown to reduce to the expected limiting cases of a shaft containing rigid appendages as the appendage's stiffness increases, and to an elastic shaft with a concentrated mass at the point of appendage attachment when the appendage's stiffness decreases. Stability boundaries are obtained by a Liapunov analysis in which the system's dynamic potential serves as a Liapunov testing function.

Analysis

Consider a simplified physical model consisting of two identical Euler-Bernoulli beam appendages rigidly attached in a normal direction to an Euler-Bernoulli shaft. The shaft is constrained between two short end bearings and rotates with constant angular speed Ω about its z axis, as shown in Fig. 1. The shaft's u and v displacement coordinates rotate with the shaft, with u taken normal to the plane defined by the shaft and beams. The primary influence of beam flexibility on whirl stability is due to the beam's η deformation in the y-z plane. Aerodynamic effects, which introduce additional stability phenomena, are neglected in order to concentrate specifically on the mechanism by which forward whirl stability can be affected by beam flexibility.

Retaining only the kinetic energy terms of zero degree in the velocity variables, the kinetic energy and bending strain energy expressions for the shaft of mass per unit length ρ, length L, and flexural rigidity EI are

$$T_s = \frac{1}{2}\int_0^L \rho\,(u^2+v^2)\Omega^2 dz \tag{1}$$

$$V_s = \frac{1}{2}\int_0^L EI\left[\left(\frac{\partial^2 u}{\partial z^2}\right)^2+\left(\frac{\partial^2 v}{\partial z^2}\right)^2\right]dz \tag{2}$$

Following the analytical method developed in Ref. 3, the corresponding kinetic energy and flexural strain energy terms for the rotating inclined radial beams, each having mass per unit volume γ, cross-sectional area A, length l, and flexural rigidity EI_η, are

$$T_b = \frac{\Omega^2}{2}\int_0^l \gamma A\left\{u^2(d)+v^2(d)-\frac{1}{2}(l^2-y^2)\left[\left(\frac{\partial\eta_1}{\partial y}\right)^2+\left(\frac{\partial\eta_2}{\partial y}\right)^2\right]-2y^2\theta_1^2-2y(\eta_1+\eta_2)\theta_1\right\}dy \tag{3}$$

Received June 10, 1977.
Index categories: Propeller and Rotor Systems; Rotating Machinery.

*Graduate Student, Engineering Mechanics Department; now at General Mills, Inc., Minneapolis, Minn. Member AIAA.
†Professor of Engineering Mechanics. Member AIAA.

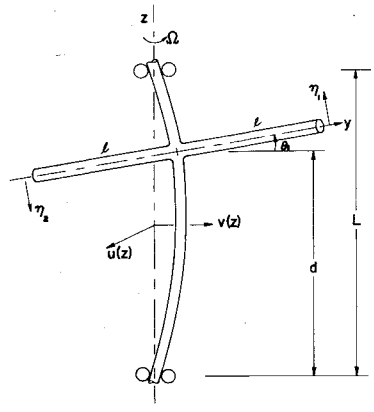

Fig. 1 Shaft beam configuration.

$$V_b = \frac{1}{2}\int_0^l EI_\eta\left[\left(\frac{\partial^2\eta_1}{\partial y^2}\right)^2+\left(\frac{\partial^2\eta_2}{\partial y^2}\right)^2\right]dy \tag{4}$$

where $\theta_1 = -\partial v(d)/\partial z$. The governing stability conditions are found to occur when $\eta_1 = \eta_2$, which is denoted subsequently by η in the following equations.

Based on the recent work of Meirovitch[4] for modal representation of rotating systems, the modal deformations of the shaft are taken in the form of the set of admissible functions

$$u(z) = \sum_{i=1}^{k} a_i \sin\left(\frac{i\pi z}{L}\right) \tag{5}$$

$$v(z) = \sum_{i=1}^{k} b_i \sin\left(\frac{i\pi z}{L}\right) \tag{6}$$

The beam's deformations are represented by the comparison function

$$\eta(y) = \eta\,[(\sin\beta l-\sinh\beta l)(\sin\beta y-\sinh\beta y) + (\cos\beta l+\cosh\beta l)(\cos\beta y-\cosh\beta y)] \tag{7}$$

where $\beta l = 1.8751$.

The dynamic equilibrium position of interest for this system occurs when $\dot{a}_i = \dot{b}_i = \dot{\eta} = a_i = b_i = \eta = 0$. Stability criteria for the system are established by determining the conditions under which the dynamic potential U is positive definite in the neighborhood of the equilibrium position, where

$$U = -(T_s+T_b)+(V_s+V_b) \tag{8}$$

Two alternative approaches are available to treat the coefficients a_i and b_i, namely, the Rayleigh-Ritz method and the method of Brown and Schlack.[5] Each can be shown to provide identical stability criteria.[6] Because of its computational advantages, the latter method, which treats each coefficient a_i, b_i, and η as independent degrees of freedom q_i, is used here.

Positive definiteness of the dynamic potential U is determined by application of Sylvester's criteria to the principle determinants of the Hessian matrix $[H]$ evaluated at the equilibrium position, where the components of H are given by

$$H_{ij} = \left.\frac{\partial^2 U}{\partial q_i \partial q_j}\right|_{\text{equilibrium}} \tag{9}$$

Denoting the mass of the shaft by M, the total mass of both beams by m, the critical speed of an elastic shaft alone by Ω_{cr}, and making appropriate algebraic modifications, the components of the Hessian matrix are obtained in dimensionless

form as

$$\frac{\partial^2 \bar{U}}{\partial a_i^2} = -1 + \frac{\Omega_{cr}^2}{\Omega^2} i^4 - 2\frac{m}{M}\sin^2\frac{i\pi d}{L} \tag{10}$$

$$\frac{\partial^2 \bar{U}}{\partial a_i \partial b_j} = \frac{\partial^2 \bar{U}}{\partial a_i \partial \eta} = \frac{\partial^2 \bar{U}}{\partial a_i \partial a_{j\neq j}} = 0 \tag{11}$$

$$\frac{\partial^2 \bar{U}}{\partial b_i^2} = -1 + \frac{\Omega_{cr}^2}{\Omega^2} i^4 - 2\frac{m}{M}\sin^2\frac{i\pi d}{L} + \frac{2}{3}\frac{m}{M}\left(i\pi\frac{l}{L}\cos\frac{i\pi d}{L}\right)^2 \tag{12}$$

$$\frac{\partial^2 \bar{U}}{\partial b_i \partial b_{j_{i\neq j}}} = -2\frac{m}{M}\sin\frac{i\pi d}{L}\sin\frac{j\pi d}{L} + \frac{2}{3}\frac{m}{M} ij\pi^2 \frac{l^2}{L^2}\cos\frac{i\pi d}{L}\cos\frac{j\pi d}{L} \tag{13}$$

$$\frac{\partial^2 \bar{U}}{\partial b_i \partial \eta} = -2\pi i \frac{m}{M}\frac{l}{L}\cos\frac{i\pi d}{L} \tag{14}$$

$$\frac{\partial^2 \bar{U}}{\partial \eta^2} = 6\frac{m}{M}\frac{\omega^2}{\Omega^2} \tag{15}$$

where

$$\omega^2 = 1.030(1.192\Omega^2 + \omega_{nr}^2) \tag{16}$$

$$\omega_{nr}^2 = (3.516)^2 EI_\eta/(l^3 m/2) \tag{17}$$

$$\Omega_{cr}^2 = \pi^4 EI/(\rho L^4) \tag{18}$$

The small coefficient in Eq. (16) is due to the expression

$$\int_0^l \eta^2 dy \Big/ \left(\sqrt{3}\int_0^l \eta y\, dy\right)^2 = 1.030 \tag{19}$$

The shaft's u-mode stability conditions are provided by the diagonal terms given by Eqs. (10) and (11) in the Hessian matrix. They are observed to uncouple from the rest of the problem and can be considered separately. These u-mode stability conditions yield the critical speeds corresponding to an elastic shaft containing a concentrated point mass m and are unaffected by beam flexibility.

The shaft's v-mode, represented by the b_i coefficients, is coupled with the beam flexibility. A measure of beam flexibility is provided by the beam's nonrotating circular natural frequency ω_{nr}. The system's v-mode stability conditions are critically dependent on the proper formulation for the beam's rotating circular natural frequency ω. Equation (16) is valid for large values of ω_{nr}/Ω. Perhaps the most accurate value of ω available in the literature for small values of ω_{nr}/Ω is given by Colin[7] as (after converting to the present notation)

$$\omega^2 = \Omega^2 + (2.121/3.516)\Omega\omega_{nr} \tag{20}$$

Recently, an expression suitable for the entire range of values for ω_{nr}/Ω was obtained by Likins et al.[8] as

$$\omega^2 \simeq \Omega^2 (1 - \tanh x/x)^{-1} \tag{21}$$

where

$$x \simeq \sqrt{3}\Omega/\omega_{nr} \tag{22}$$

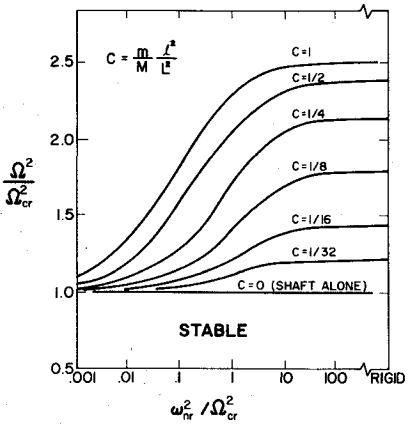

Fig. 2 Stability boundaries for $d/L = 1$.

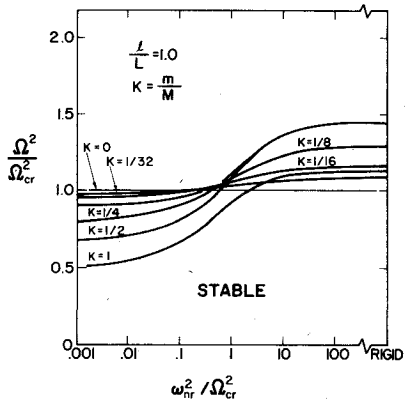

Fig. 3 Stability boundaries for $d/L = 3/4$.

The v-mode stability boundaries obtained from using 10 terms from Eqs. (12–15) and (21) are shown in Figs. 2 and 3. Figure 2 provides stability boundaries as a function of beam flexibility for beams of a variety of sizes which are attached to the shaft at $d/L = 1$, and Fig. 3 at $d/L = 3/4$. For $d/L = 1/2$, gyroscopic moment contributions from the cosine components in Eqs. (12–15) vanish, and these boundaries reduce to straight lines independent of appendage flexibility. Although a single sine term is sufficient to represent a shaft with small appendages, as many as 10 terms are required to obtain suitable stablity boundary convergence for the larger appendages. The stability boundaries are bounded above by the critical speed of a shaft with rigid beams, and below by the critical speed of a shaft with a concentrated mass m at the point of beam attachment.

Valuable insight into the nature of the effect of flexibility on stability is obtained from examination of the single sine term stability condition given by

$$1 - \frac{\Omega^2}{\Omega_{cr}^2} - 2\frac{m}{M}\frac{\Omega^2}{\Omega_{cr}^2}\sin^2\frac{\pi d}{L} + \frac{2}{3}\frac{m}{M}\left(\pi\frac{l}{L}\frac{\Omega}{\Omega_{cr}}\cos\frac{\pi d}{L}\right)^2\left(1 - \frac{\Omega^2}{\omega^2}\right) > 0 \tag{23}$$

The individual terms in Eq. (23) can be identified as stability contributions due to an elastic shaft alone, a concentrated mass, a gyroscopic moment due to rigid beams, and beam flexibility, respectively. Using the appropriate value of ω^2 in Eqs. (16) and (20) for large and small values of ω_{nr}, Eq. (23) reduces to the proper special cases. These special cases can be visualized as represented by a shaft with rigid appendages and rope-type appendages, respectively. More detailed considerations of this model, as well as the more complex disk appendage model for which similar results are obtained, are available in Ref. 6.

References

[1] Chivens, D.R. and Nelson, H.D., "The Natural Frequencies and Critical Speeds of a Rotating, Flexible Shaft-Disk System," *Journal of Engineering for Industry*, Vol. 97, Ser. B, Aug. 1975, pp. 881-886.

[2] Klompas, N., "Theory of Rotor Dynamics with Coupling of Disk and Blade Flexibility and Support Structure Asymmetry," *ASME Gas Turbine Conference and Products Show*, ASME Paper 74-GT-159, Zurich, Switzerland, March 30-April 4, 1974.

[3] Vigneron, F.R., "Comment on 'Mathematical Modeling of Spinning Elastic Bodies for Modal Analysis,' " *AIAA Journal*, Vol. 13, Jan. 1975, pp. 126-127.

[4] Meirovitch, L., "A Stationarity Principle for the Eigenvalue Problem for Rotating Structures," *AIAA Journal*, Vol. 14, Oct. 1976, pp. 1387-1394.

[5] Brown, D.P. and Schlack, A.L., Jr., "Stability of a Spinning Body Containing an Elastic Membrane via Liapunov's Direct Method," *AIAA Journal*, Vol. 10, Oct. 1972, pp. 1286-1290.

[6] Wilgen, F.J., "The Effect of Appendage Flexibility on Shaft Whirl Stability," Ph.D. Dissertation, Dept. of Engineering Mechanics, Univ. of Wisconsin, Madison, Wisc., 1977.

[7] Colin, A.D., "Modal Analysis for Liapunov Stability of Rotating Elastic Bodies," Ph.D. Dissertation, Engineering-Aeronautical, Univ. of California, Los Angeles, Calif., 1973.

[8] Likins, P.W., Barbera, F.J., and Baddeley, V., "Mathematical Modeling of Spinning Elastic Bodies for Modal Analysis," *AIAA Journal*, Vol. 11, Sept. 1973, pp. 1251-1258.

A Paradoxical Case in a Stability Analysis

R. Parnes*

Tel-Aviv University, Ramat-Aviv, Israel

In analyzing elastic systems subjected to compressive loads, it is generally accepted that the load at which instability occurs decreases as the member increases in length. In the model investigated below, the opposite is found to be true. Aside from its academic interest, the implications of the behavior of the given model may be of some significance, for example, in the design of prostheses.

Consider the model shown in Fig. 1a, where EI and $E'I' = \alpha^2 EI$ are the flexural rigidities of members AB and BC, respectively, and where L and cL are the respective lengths. From stability theory, one might conclude that the axial load P at which instability occurs decreases for all increasing values of the parameter $c>0$. However, as is shown below, such behavior exists only within a range $c_0<c$, where c_0 is a constant dependent on α. Paradoxically, for values $c<c_0$, increasing the length of the member *increases* the buckling load.

We first consider the simpler case where member BC is infinitely rigid i.e., $E'I' \to \infty$ or $\alpha \to \infty$. The resulting neutral equilibrium position in the deformed state is as shown in Fig. 1b, where $\Delta = v(L)$ is a small displacement.

The corresponding eigenvalue problem then consists of the equilibrium equation

$$\frac{d^2v(x)}{dx^2} + \beta^2 v(x) = \beta^2 \Delta\left[1 + \frac{1}{c} - \frac{x}{cL}\right] \tag{1}$$

and the boundary conditions

$$v(0) = \frac{dv(0)}{dx} = 0, \quad v(L) = \Delta \tag{2}$$

Received May 27, 1977.

Index categories: Structural Design; Structural Stability.

*Associate Professor, Department of Solid Mechanics, Materials and Structures, School of Engineering.

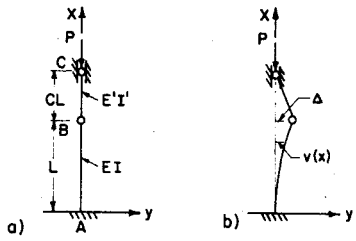

Fig. 1 Geometry of problem.

where

$$\beta^2 = P/EI \tag{3}$$

Solutions of this boundary-value problem lead to eigenvalues that are the roots of the equation

$$f(\beta L) \equiv \tan\beta L - (1+c)\beta L = 0 \tag{4}$$

It is recognized that, when $c=0$, we recover the known transcendental equation for a member fixed at one end and hinged at the other, while as $c \to \infty$ we obtain the equation $\cos\beta L = 0$, which corresponds to a cantilevered-free end member subject to an axial load, where the smallest load of instability is the classical value[1]

$$P_E = \pi^2 EI/4L^2 \tag{5}$$

For the problem at hand, the loads causing instability, obtained from Eq. (4), are plotted in nondimensional form P/P_E as a function of the parameter c (solid line) in Fig. 2. It is noted that, as $c \to 0$, the value of P approaches zero, whereas for all $c \to \infty$ the value $P \to P_E$ asymptotically. Thus, for increasing lengths of cL, the load P required to cause instability actually increases; the value c_0, as previously defined, is infinite.

The usual behavior of small values of c now can be examined more closely. It is evident that, when $c=0$ identically, we obtain from Eq. (4) the classical value[1]

$$P \doteq [\pi^2 EI/(0.7L)^2] > P_E \tag{6}$$

although Fig. 2 indicates values approaching zero.

The apparent discrepancy may be explained by considering the graph of Fig. 3, showing the roots of Eq. (4). It is realized immediately that, for $c=0$, the relevant root is given by point A, whereas for any $c>0$ the relevant root is represented by the generic point B, which lies on a different branch. As $c \to \infty$, again $\beta L \to \pi/2$, and thus $P/P_E \to 1$, as shown in Fig. 2.

In the preceding analysis, member BC was assumed rigid for mathematical simplicity. If we return to the problem where member BC has a finite flexural rigidity $E'I' = \alpha^2 EI$, we obtain, in lieu of Eq. (4), the uncoupled equation

$$\sin(\beta cL/\alpha)[\tan\beta L - (1+c)\beta L] = 0 \tag{7}$$

The roots of this equation are clearly the same as those obtained previously from $f(\beta L) = 0$, with additional roots from the equation

$$\sin(\beta cL/\alpha) = 0 \tag{8}$$

which correspond to the instability of member BC considered as a pin-connected member. The actual load causing instability is then the smaller of the two roots given by Eq. (4) or (8), depending on the relative geometry and stiffnesses, i.e., on the parameters c and α. The nondimensional instabilitiy loads P/P_E are plotted as a function of c in Fig. 2, where the dashed lines, representing the loads corresponding to the roots of Eq. (8) for the family of curves of α, are given by

$$P/P_E = 4\alpha^2/c^2 \tag{9}$$